PNAS BRIEF REPORT | EARTH, ATMOSPHERIC, AND PLANETARY SCIENCES OPEN ACCESS

Simulating atmospheric freezing of single aqueous droplets to ice in a cryogenically cooled ultrasonic levitator

Souvick Biswas[a], Dababrata Paul[a], Koushik Mondal[a], and Ralf I. Kaiser[a,1]

Edited by Catherine Murphy, University of Illinois at Urbana-Champaign, Urbana, IL; received December 8, 2024; accepted January 8, 2025

Atmospheric freezing of water droplets suspended in air followed by cloud formation and precipitation represent fundamental steps of the terrestrial water cycle. These aqueous droplets exhibit distinct freezing mechanisms and thermodynamic requirements compared to bulk water often forming metastable supercooled water at subzero temperatures on the Celsius scale (<273 K) prior to crystallization. Here, we report on a real-time spectroscopic investigation combined with simultaneous visualizations of single aqueous droplet freezing events inside a cryogenically cooled ultrasonic levitation chamber with the ultimate goal of probing the molecular structure evolution and stages of ice formation. The observed droplet freezing follows a pseudoheterogeneous ice nucleation mechanism mimicking the process that occurs for atmospherically supercooled water droplets at the air–water interface. This proof-of-concept experimental setup allows future crystallization studies of homo- and heterogeneously doped aqueous droplets under simulated atmospheric environments—also in the presence of reactive trace gases, thus untangling dynamic molecular interactions and chemical reactions, which are of fundamental interest to low-temperature atmospheric chemistry delineating with ice nucleation mechanisms.

droplet freezing | cryogenic cooling | ice nucleation | simulation chamber | Raman spectroscopy

The freezing of water droplets to ice is ubiquitous in nature and plays a central role in fundamental atmospheric processes such as cloud formation and precipitation including snow and hail (Fig. 1). During the upward transport, water vapor condenses to droplets which continue to cool down below the freezing point of water (273 K) reaching a metastable state referred to as supercooled water; these undergo ice nucleation attaining the crystalline solid state—a pivotal step that has long piqued the interest of the scientific communities in chemistry, physics, and atmospheric sciences (1, 2). Prior experiments reveal that the freezing phenomenon largely depends on the sizes of aqueous droplets and the surrounding conditions (3–7). In most of the cases, the droplet was cooled on a macroscopic surface, where the contact effect could essentially trigger the ice nucleation (8, 9). Moreover, the majority of the studies have been performed under a vacuum for a spectroscopic characterization (10, 11). In these circumstances, fast freezing events at extremely low temperatures down to 173 K are frequently reported in the literature, which differ from the actual atmospheric situation (12, 13).

Here, we report the combined time-dependent spectroscopic and high-speed imaging investigation of an acoustically levitated single water droplet freezing to ice inside a newly home-built cryogenically cooled process chamber thus eliminating any surface effects to reveal the temporal evolution of the molecular structure along with distinct stages of the cooling process. Atmospherically relevant conditions are simulated in the process chamber (Fig. 2*A* and *SI Appendix*) starting with, e.g., tropospheric pressure ranges (760 ± 10 Torr), and as a case study for chemically inert dry nitrogen (N_2) environments. The temperature of the simulated atmosphere inside the chamber and its spatial variation is monitored by a flexible silicon diode temperature sensor, while the accurate temperature of the aqueous droplet/ice particle is probed by an infrared camera (*SI Appendix*).

Results and Discussion

The water droplet is introduced to the second pressure node into the process chamber through a microneedle mounted on a wobble stick and undergoes freezing via distinct steps as the temperature drops (Fig. 2*B* and Movie S1). For a typical 1-μL-sized levitated droplet, the opacity changed at a temperature of 270.9 ± 0.5 K just below the freezing point of water indicating a shift in density and initiating the formation of ice nuclei. However, the droplet held its fluid nature and revealed a metastable supercooled water until reaching the temperature of 268.9 ± 0.7 K while forming an ice crust followed by inward dendritic ice growth to the liquid core. This process represents the

Author affiliations: [a]Department of Chemistry, University of Hawai'i at Manoa, Honolulu, HI 96822

Author contributions: S.B. and R.I.K. designed research; S.B., D.P., and K.M. performed research; S.B. analyzed data; R.I.K. supervised and edited paper; and S.B. wrote the paper.

The authors declare no competing interest.

[1]To whom correspondence may be addressed. Email: ralfk@hawaii.edu.

This article contains supporting information online at https://www.pnas.org/lookup/suppl/doi:10.1073/pnas.2425543122/-/DCSupplemental.

Published February 3, 2025.

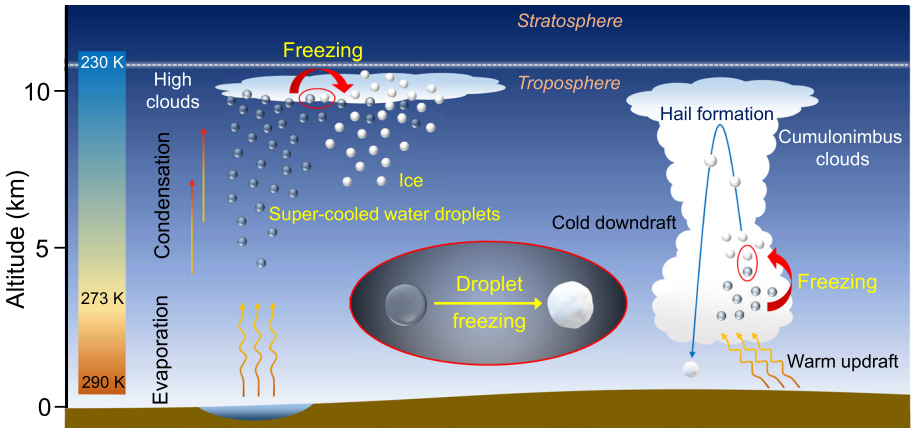

Fig. 1. Natural atmospheric processes involving freezing of water droplets to ice as a key step.

droplet surface-induced *ice* nucleation at the interface of water and cooled nitrogen buffer gas. A small rise of droplet temperature was noted up to 269.8 ± 0.7 K due to dissipation of the latent heat from freezing. Subsequently, the droplet was rapidly transformed into a slushy ice particle, which solidified to ice at 268.5 ± 0.7 K. This process is accompanied by a slight volume increase compared to the levitated water droplet as visible. A correlation of the freezing point with droplet volume reveals a decreasing trend of the freezing point with the droplets increasing in size (Fig. 2*D*). The relative humidity of the simulated atmosphere across the temperature range was negligible to have any significant effect on the freezing process of levitated droplet (*SI Appendix*).

Time-dependent Raman spectra (Fig. 2*E*) track the temporal changes in the molecular arrangements during the freezing process by revealing significant spectral alterations. First, the overall band shape of the dangling O—H stretching frequency region (ν_{OH}: 3,800 to 2,800 cm^{-1}) evolved with a sharp and prominent band in the crystalline ice (hexagonal, I_h) (3,144 cm^{-1}) (14) which is redshifted from the 3,224 cm^{-1} band, i.e., the O—H stretch ($\nu_{OH\text{-}DDAA}$) of the tetrahedrally hydrogen bonded water molecule with double donor-double acceptor (DDAA) configuration in the pentameric unit (14–16). This phenomenon is attributed to considerably stronger and more complex hydrogen bonding in the ice structure. However, O—H stretching vibrations of water and ice are very sensitive to their local environment with strong

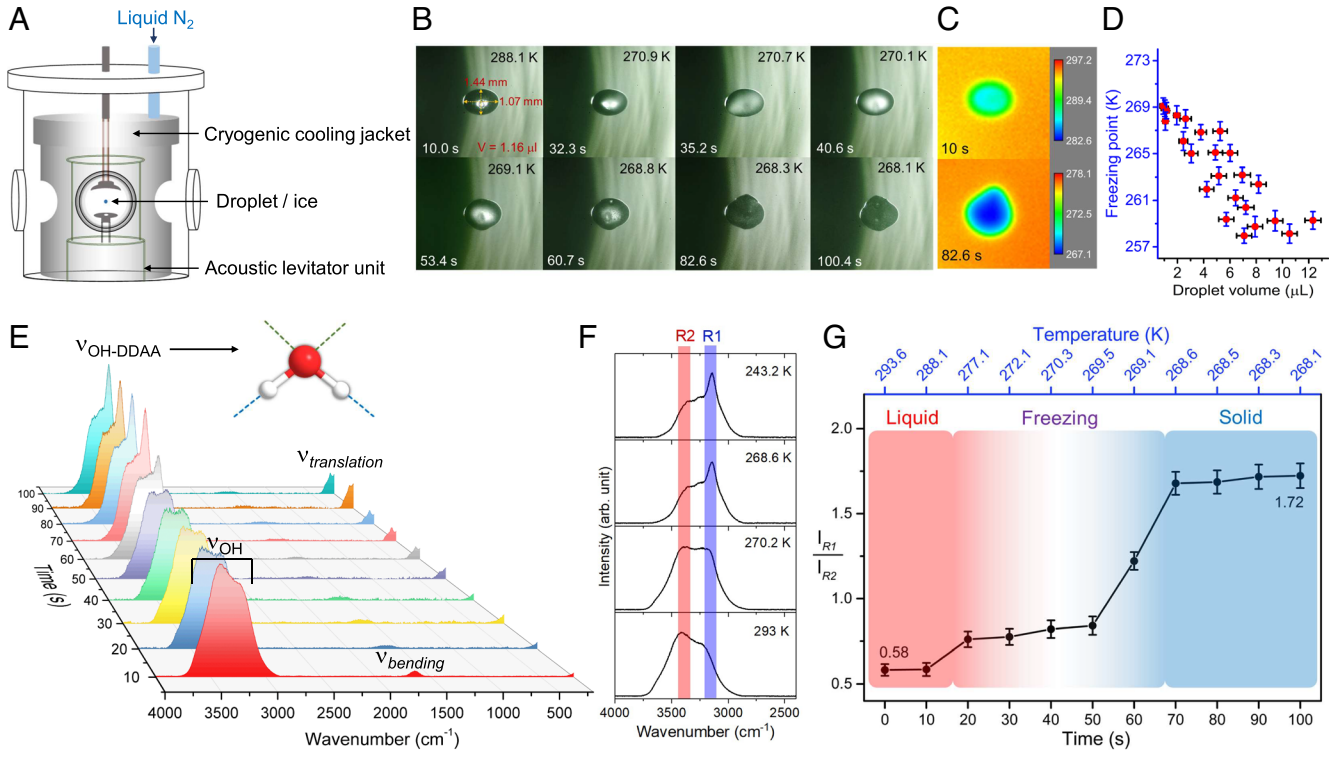

Fig. 2. (*A*) Schematic of the process chamber with a cryogenic cooling jacket surrounding the acoustic levitator unit. (*B*) Visualization of the freezing process of levitating water droplet with temperature and time. (*C*) Representative thermal images of the water droplet and ice particle. (*D*) Freezing point as a function of droplet volume. (*E*) Time-dependent Raman spectra tracing the change in the physical state and molecular structure of water during freezing. The broad spectral region 3,800 to 2,800 cm^{-1} corresponds to the O—H stretching frequencies arising out of different kinds of intermolecular interactions. The sharp $\nu_{OH\text{-}DDAA}$ band of ice represents the coupled O—H stretching of pentameric tetrahedral molecular arrangement of water with double donor-double acceptor (DDAA) hydrogen bond linkages. (*F*) The freezing process is quantified by evaluating the ratios of corresponding areas of two spectral segments from 3,200 to 3,100 cm^{-1} (R1) and 3,440 to 3,340 cm^{-1} (R2) representing the typical vibrational features for ice and liquid water, respectively. (*G*) Temporal profile of the water droplet freezing process along with droplet/ice temperature.

coupling of intramolecular and intermolecular vibrations. Therefore, spectral interpretation in terms of the normal modes, i.e., molecular symmetric and antisymmetric stretches, are fundamentally inappropriate; instead, they are assigned based on localized O—H stretches. The interplay of such O—H stretches pertaining to dynamic molecular structures is evident from the gradual changes in the relative intensities of the 3,224 cm^{-1} ($\nu_{OH\text{-}DDAA}$) and 3,430 cm^{-1} ($\nu_{OH\text{-}DDA;}$ DDA: double donor-single acceptor) bands. Both undergo spectral redshifts by 80 and 66 cm^{-1}, respectively, while cooling from 293.6 ± 0.9 K to 268.5 ± 0.7 K. In between 20 and 50 s, these bands, which represent supercooled water, are nearly equal in intensity, whereas beyond 60 s, the 3,144 cm^{-1} band becomes predominant implying ice formation. The diminished intensity of the redshifted $\nu_{OH\text{-}DDA}$ band (3,364 cm^{-1}) in ice also indicates a structural reorganization in the bilayer framework compared to liquid water (17). Second, a remarkable intensity reduction of the bending mode (1,645 cm^{-1}) upon crystallization is evident; this phenomenon owes to the loss of induced transition dipole moment suggesting that the concerned vibration primarily reflects water molecules that do not conform to symmetric tetrahedral environment in the liquid phase. Third, the appearance of structured bands at low-frequency range below 370 cm^{-1} for ice is linked to intermolecular O…H vibrational modes, namely hindered translations of water molecules in the rigid H-bonded network.

The temporal evolution of spectrally rich ν_{OH} bands upon cooling depicts that the features below the 3,300 cm^{-1} band are enhanced, while those above 3,300 cm^{-1} get diminished due to overall alteration in structural motifs and strengthened intermolecular interactions thus weakening O—H bonds. Hence, the aforesaid spectral segments, in particular 3,200 to 3,100 cm^{-1} (R1) and 3,440 to 3,340 cm^{-1} (R2) can be designated as characteristic features of ice and water, respectively (Fig. 2*F*). The ratio of the integral areas under these selections enables a quantification for the progress of the freezing process (Fig. 2*G*) and avoids tedious spectral deconvolutions and consequences related to small wavenumber shifts. The resulting curve with respect to time and temperature detects the actual moment of phase change, for instance, the representative mean ratio for supercooled water (t = 20 to 50 s) is 0.81 ± 0.07, slightly elevated than liquid water at 293 K (0.58 ± 0.04), while the bulk ice formation (dendritic growth) is triggered at ~60 s as evidenced from the inflection point of the curve (1.22 ± 0.07) until reaching the I_h ice at 70 s onward (1.68 ± 0.07). The temperature-dependent temporal curve functions as a spectral marker that accurately identifies the phases and freezing point of water versus ice.

In conclusion, this study utilizing a recently developed cryogenically cooled ultrasonic levitator in a simulated environment, combined with real-time Raman spectroscopy and simultaneous visualization techniques, provides a molecular-level understanding of the freezing process for aqueous droplets by identifying the critical steps of supercooling, droplet surface-induced ice nucleation at the buffer gas–water interface, dendritic ice growth, and complete freezing. This study represents the very first of its kind, where future crystallization studies will use aqueous solutions doped with atmospherically relevant liquids and solids, further mixing reactive pollutant gases with the buffer gas to identify the precise physicochemical effects on ice nucleation processes. Controlling the buffer gas temperature, pressure, chemical composition, and constituent(s) of levitating liquid or solid sample, the apparatus can be expanded to planetary astrochemistry beyond terrestrial atmospheric chemistry.

Materials and Methods

The aqueous droplets were levitated at the stable pressure node in a 58 kHz ultrasonic levitator surrounded by a cooling jacket filled with liquid nitrogen. Visuals and droplet temperatures were recorded by high-speed optical and infrared cameras, respectively. The temperature of the experimental environment was monitored with a silicon diode sensor. Raman spectra were obtained by exciting the sample with a 532 nm diode-pumped, Q-switched Nd:YAG laser and collecting signal via a holographic imaging spectrograph equipped with an intensified charge-coupled device (ICCD). The detailed experimental method may be found in *SI Appendix*.

Data, Materials, and Software Availability. All study data are included in the article and/or supporting information.

ACKNOWLEDGMENTS. The assembly of the cooled setup was funded by NASA under grant 80NSSC22K0976; the experiments were funded through the NSF award, 2330175, Center: NSF Engineering Research Center for Environmentally Applied Refrigerant Technology Hub.

1. D. A. Knopf, P. A. Alpert, Atmospheric ice nucleation. *Nat. Rev. Phys.* **5**, 203–217 (2023).
2. E. B. Moore, V. Molinero, Structural transformation in supercooled water controls the crystallization rate of ice. *Nature* **479**, 506–508 (2011).
3. N. Shardt *et al.*, Homogeneous freezing of water droplets for different volumes and cooling rates. *Phys. Chem. Chem. Phys.* **24**, 28213–28221 (2022).
4. H. Jingru, L. Jingbin, H. Zhongwei, C. Kang, X. Haojun, Experimental study on the freezing process of water droplets for ice air jet technology. *Sci. Rep.* **14**, 3259 (2024).
5. T. Buttersack, S. Bauerecker, Critical radius of supercooled water droplets: On the transition toward dendritic freezing. *J. Phys. Chem. B* **120**, 504–512 (2016).
6. N. J. Mason *et al.*, The spectroscopy and chemical dynamics of microparticles explored using an ultrasonic trap. *Faraday Discuss.* **137**, 367–376 (2008).
7. A. McElligott *et al.*, TinyLev acoustically levitated water: Direct observation of collective, inter-droplet effects through morphological and thermal analysis of multiple droplets. *J. Colloid Interface Sci.* **619**, 84–95 (2022).
8. B. J. Murray *et al.*, Kinetics of the homogeneous freezing of water. *Phys. Chem. Chem. Phys.* **12**, 10380–10387 (2010).
9. S. Wildeman, S. Sterl, C. Sun, D. Lohse, Fast dynamics of water droplets freezing from the outside in. *Phys. Rev. Lett.* **118**, 084101 (2017).
10. A. Kalita *et al.*, Microstructure and crystal order during freezing of supercooled water drops. *Nature* **620**, 557–561 (2023).
11. A. Manka *et al.*, Freezing water in no-man's land. *Phys. Chem. Chem. Phys.* **14**, 4505–4516 (2012).
12. G. A. Kimmel *et al.*, Homogeneous ice nucleation rates and crystallization kinetics in transiently-heated, supercooled water films from 188 K to 230 K. *J. Chem. Phys.* **150**, 204509 (2019).
13. Y. Yao, C. Li, Z. Tao, R. Yang, H. Zhang, Experimental and numerical study on the impact and freezing process of a water droplet on a cold surface. *Appl. Therm. Eng.* **137**, 83–92 (2018).
14. Q. Sun, H. Zheng, Raman OH stretching vibration of ice Ih. *Prog. Nat. Sci.* **19**, 1651–1654 (2009).
15. L. Shi, S. M. Gruenbaum, J. L. Skinner, Interpretation of IR and raman line shapes for H_2O and D_2O Ice Ih. *J. Phys. Chem. B* **116**, 13821–13830 (2012).
16. W. J. Smit *et al.*, Observation and identification of a new OH stretch vibrational band at the surface of ice. *J. Phys. Chem. Lett.* **8**, 3656–3660 (2017).
17. M. A. Sánchez *et al.*, Experimental and theoretical evidence for bilayer-by-bilayer surface melting of crystalline ice. *Proc. Natl. Acad. Sci. U.S.A.* **114**, 227–232 (2017).